



**HAL**  
open science

## **Saturn's Northern Aurorae at Solstice From HST Observations Coordinated With Cassini's Grand Finale**

L. Lamy, R. Prangé, C. Tao, T. Kim, S. V. Badman, P. Zarka, B. Cecconi, W.  
S. Kurth, W. Pryor, E. Bunce, et al.

► **To cite this version:**

L. Lamy, R. Prangé, C. Tao, T. Kim, S. V. Badman, et al.. Saturn's Northern Aurorae at Solstice From HST Observations Coordinated With Cassini's Grand Finale. *Geophysical Research Letters*, 2018, 45 (18), pp.9353-9362. 10.1029/2018GL078211 . hal-01952976

**HAL Id: hal-01952976**

**<https://hal.sorbonne-universite.fr/hal-01952976>**

Submitted on 7 Jan 2022

**HAL** is a multi-disciplinary open access archive for the deposit and dissemination of scientific research documents, whether they are published or not. The documents may come from teaching and research institutions in France or abroad, or from public or private research centers.

L'archive ouverte pluridisciplinaire **HAL**, est destinée au dépôt et à la diffusion de documents scientifiques de niveau recherche, publiés ou non, émanant des établissements d'enseignement et de recherche français ou étrangers, des laboratoires publics ou privés.

Copyright

## RESEARCH LETTER

10.1029/2018GL078211

## Special Section:

Cassini's Final Year: Science Highlights and Discoveries

## Key Points:

- Saturn's northern UV aurorae at solstice were sampled from HST observations coordinated with Cassini's Grand Finale
- The observed aurorae are highly variable with powerful events, radiating up to 124 GW, controlled by solar wind and planetary rotation
- The average auroral brightness strongly varies with LT with two maxima at dawn (previously known) and premidnight (newly identified)

## Supporting Information:

- Supporting Information S1
- Movie S1
- Figure S1
- Figure S2
- Figure S3
- Figure S4
- Figure S5

## Correspondence to:

L. Lamy,  
laurent.lamy@obspm.fr

## Citation:

Lamy, L., Prangé, R., Tao, C., Kim, T., Badman, S. V., Zarka, P., et al. (2018). Saturn's northern aurorae at solstice from HST observations coordinated with Cassini's grand finale. *Geophysical Research Letters*, 45, 9353–9362. <https://doi.org/10.1029/2018GL078211>

Received 9 APR 2018

Accepted 7 JUL 2018

Accepted article online 17 JUL 2018

Published online 23 SEP 2018

# Saturn's Northern Aurorae at Solstice From HST Observations Coordinated With Cassini's Grand Finale

 L. Lamy<sup>1</sup> , R. Prangé<sup>1</sup>, C. Tao<sup>2</sup> , T. Kim<sup>3</sup> , S. V. Badman<sup>4</sup> , P. Zarka<sup>1</sup> , B. Cecconi<sup>1</sup> ,  
 W. S. Kurth<sup>5</sup> , W. Pryor<sup>6</sup> , E. Bunce<sup>7</sup> , and A. Radioti<sup>8</sup>

<sup>1</sup>LESIA, Observatoire de Paris, PSL, CNRS, UPMC, Université Paris Diderot, Meudon, France, <sup>2</sup>National Institute of Information and Communications Technology, Tokyo, Japan, <sup>3</sup>Center for Space Plasma and Aeronomic Research, University of Alabama, Huntsville, AL, USA, <sup>4</sup>Department of Physics, Lancaster University, Lancaster, UK, <sup>5</sup>Department of Physics and Astronomy, University of Iowa, Iowa City, IA, USA, <sup>6</sup>Department of Science, Central Arizona College, Coolidge, AZ, USA, <sup>7</sup>Department of Physics and Astronomy, University of Leicester, Leicester, UK, <sup>8</sup>Space Science, Technologies and Astrophysics Research Institute, Liège, Belgium

**Abstract** Throughout 2017, the Hubble Space Telescope (HST) observed the northern far-ultraviolet aurorae of Saturn at northern solstice, during the Cassini Grand Finale. These conditions provided a complete viewing of the northern auroral region from Earth and a maximal solar illumination, expected to maximize the ionosphere-magnetosphere coupling. We analyze 24 HST images concurrently with Cassini measurements of Saturn's kilometric radiation and solar wind parameters predicted by two magnetohydrodynamic models. The aurorae reveal highly variable components, down to timescales of minutes, radiating 7 to 124 GW. They include a nightside-shifted main oval, unexpectedly frequent and bright cusp emissions, and a dayside low-latitude component. On average, these emissions display a strong local time dependence with two maxima at dawn and premidnight, the latter being newly observed and attributed to nightside injections possibly associated with solstice conditions. These results provide a reference frame to analyze Cassini in situ measurements, whether simultaneous or not.

**Plain Language Summary** In 2017, the Hubble Space Telescope regularly observed the northern ultraviolet aurorae of Saturn in coordination with Cassini in situ measurements obtained during the Grand Finale, when the spacecraft flew across magnetic field lines connected to the aurorae. Hubble imaged Saturn's aurorae at 24 occasions spread over 7 months during northern solstice, when the northern auroral region was both fully visible from Earth and permanently illuminated by the Sun. The observed aurorae display a variety of components observed poleward of 68° latitude with different properties, some of which were unreported before. These emissions strongly vary with time, down to a few minutes, and radiate from 7 to 124 GW. On average, the auroral intensity also strongly varies with local time (a Sun-referenced frame) and peaks at dawn, as previously observed, and also premidnight, pointing to a recurrent nightside activity of the magnetosphere. These results provide a reference basis to analyze Cassini in situ measurements.

## 1. Introduction

Saturn's aurorae have been intensively observed from Earth with the Hubble Space Telescope (HST) in the Far-Ultraviolet (FUV) mainly using the Space Telescope Imaging Spectrograph (STIS) and the Advanced Camera for ACS). Many of these observations were coordinated with in situ measurements from the Cassini spacecraft, including its Ultraviolet Imaging Spectrometer (UVIS), during its orbital tour from 2004 to 2017. Recent reviews summarize our current understanding of kronian auroral processes (Badman et al., 2015; Kurth et al., 2009).

The UV aurorae are the neutral atmospheric response of the prominent H and H<sub>2</sub> species to precipitations of electrons energized in the magnetosphere. The energy of primary electrons, measured by various methods based on spectroscopic HST/STIS and Cassini/UVIS measurements, ranges from a few kiloelectron volts (keV) to a few tens of keV (Gustin et al., 2017). The kronian aurorae decompose into a variety of components, tentatively listed by Grodent (2015), driven by different acceleration processes and underlying current systems. We hereafter restrict ourselves to four broad categories.

The dominant auroral emission is a circumpolar main oval, whose intensity and location significantly vary with time. It was early found to be associated with auroral Saturn's Kilometric Radiation (SKR; Kurth et al., 2005) and with strong upward field-aligned currents located slightly equatorward of the open-closed field line boundary (Belenkaya et al., 2008; Bunce et al., 2008; Hunt et al., 2015). It typically radiates a few tens of kilorayleighs (kR, local photon flux per pixel) and a few tens of gigawatts (GW, total power radiated by the whole auroral region), although differing definitions of these quantities used in the literature prevent us from cross comparing them. The quiet main oval is a quasi-circular narrow faint ring of emission near  $72\text{--}75^\circ$  northern latitudes. By contrast, magnetospheric compressions driven by interplanetary shocks trigger bright auroral storms typically lasting for  $\sim 1.5$  planetary rotations ( $1.5 \times \sim 10.7$  hr), with a significant part of the main oval expanding toward high latitudes (Clarke et al., 2005, 2009; Meredith, Alexeev, et al., 2014; Prangé et al., 2004). Longitudinally extended intensifications along the undisturbed oval phased with SKR periodic bursts were alternately related to rotationally modulated nightside injections (Jackman et al., 2009; Lamy et al., 2013; Mitchell et al., 2009; Nichols, Cecconi, et al., 2010). The main oval additionally hosts a variety of smaller-scale transient and/or subcorotating hot spots (Grodent et al., 2011; Meredith et al., 2013; Radioti, 2009, 2015). On average, its brightness strongly varies with local time (LT) with a main maximum at dawn (Carbary, 2012; Lamy et al., 2009, and references therein), a peculiarity of Saturn's aurorae.

Cusp aurorae have also been occasionally identified as emissions radiating a few GW and up to 50 kR, varying on timescales of hours, and confined close to noon either along the main oval or poleward of it depending on the orientation of the interplanetary magnetic field (Gérard et al., 2005; Kinrade et al., 2017; Meredith, Cowley, & Nichols, 2014; Palmaerts et al., 2016). Such signatures are sometimes associated with duskside bifurcations of the main emission, similarly attributed to dynamical dayside reconnection (Radioti et al., 2011). A faint secondary oval,  $\sim 2$  kR bright, has also been identified on the southern nightside in HST/STIS and then Cassini/UVIS images equatorward of the main one (Grodent et al., 2010; Lamy et al., 2013; Radioti et al., 2017). It appeared as a few degrees-wide ring near  $-67^\circ$  southern latitude, which Grodent et al. (2010) attributed to the precipitation of suprathermal electrons from the middle magnetosphere rather than to a field-aligned current system. Finally, a last important auroral feature consists of a spot at the magnetic footprint of Enceladus driven by the planet-satellite interaction. It was identified as a 1 kR bright emission near  $+64.5^\circ$  latitude in only three Cassini/UVIS images so far (Pryor et al., 2011).

In the frame of Cassini's Grand Finale, HST/STIS regularly observed Saturn's northern aurorae throughout 2017, during northern summer solstice (reached on 24 May). These conditions offered the best achievable HST viewing of the northern auroral region. They also provided maximal solar illumination, that is, maximal northern ionospheric conductivity and thus maximized ionosphere-magnetosphere coupling through the current systems driving most of the kronian aurorae. The HST observations were carefully coordinated with in situ measurements of the Cassini spacecraft within the auroral region. In this article, we analyze 24 HST/STIS images concurrently with Cassini SKR observations and propagated solar wind (SW) parameters. The data set is presented and analyzed in sections 2 and 3. Results are then discussed in section 4. Details on the HST data processing and supporting information figures are provided in the supporting information.

## 2. Data Set

### 2.1. HST/STIS Observations

During the Cassini's Grand Finale, STIS observed Saturn's far-ultraviolet auroral emissions during 25 HST orbits distributed throughout 2017. These were scheduled when Cassini was planned to traverse SKR sources, themselves collocated with layers of auroral field-aligned upward currents (Lamy et al., 2018). Each orbit included one  $\sim 44$ -min long time-tagged exposure. The time-tag mode provides the arrival time of photons recorded on the STIS multianode microchannel array detector at a  $125\text{-}\mu\text{s}$  resolution and thus enables us to track dynamics at timescales shorter than the exposure (see supporting information Figure S1 and Movie S1). Out of 25 orbits, 24 acquired  $1024 \times 1024$  pix images at  $0.00247$  arcsec/pix resolution with the Strontium Fluoride filter F25SrF<sub>2</sub> (148-nm central wavelength, 28-nm full width at half maximum) which rejects wavelengths shortward of 128 nm and notably the H Ly- $\alpha$  line. One orbit was also used to slew the northern auroral region with the 0.5 arcsec slit and the G140L grating. In this study, we focus on the analysis of the images, processed and translated into brightnesses and power radiated over the 70- to 180-nm H<sub>2</sub> bands (see supporting information).

## 2.2. Cassini/RPWS Data and SW Models

Cassini quasi-continuous observations of the Radio and Plasma Wave Science (RPWS) experiment (Gurnett et al., 2004) were used to monitor the SKR activity between a few (kHz) and  $\sim 1100$  kHz. We derived flux densities normalized to 1 AU observing distance and power integrated over 10–1100 kHz for comparison purposes with previous studies (e.g., Lamy et al., 2008). The normalization assumes a source-observer distance equal to the planet-observer one, an assumption which is less and less valid for closer Cassini-Saturn distances but fair enough to assess typical intensities. We also used northern SKR phases, derived as described in (Lamy, 2011) from the most recent northern SKR period ( $\sim 10.8$  hr throughout 2017; Lamy, 2017).

SW parameters were numerically propagated from the Earth's orbit out to Saturn with two magnetohydrodynamic codes. The Tao 1-D model was developed for the Jovian case (Tao et al., 2005) and extrapolated to Saturn's orbit (e.g., Kimura et al., 2013). The (MS-FLUKSS) (Pogorelov et al., 2014) is a 3-D model validated in the outer heliosphere thanks to in situ plasma measurements of Ulysses, Voyager, and New Horizons (Kim et al., 2016). The input parameters are, for both models, near-Earth SW in situ observations provided by either 1-hr averaged data obtained from Wind measurements (King & Papitashvili, 2005) or Stereo-A measurements instead. The uncertainty depends on the derived parameters and on the angular separation between the Earth and Saturn and gradually increases from opposition. For angular separations less than  $90^\circ$ , which provided a fair coverage of 2017 through complementary Wind and Stereo-A inputs, the typical uncertainty on the timing of dynamic pressure fronts is estimated to be less than  $\pm 35$  hr, according to previous results from another 1-D model (Zieger & Hansen, 2008), whose results were not available for this study.

## 3. Results

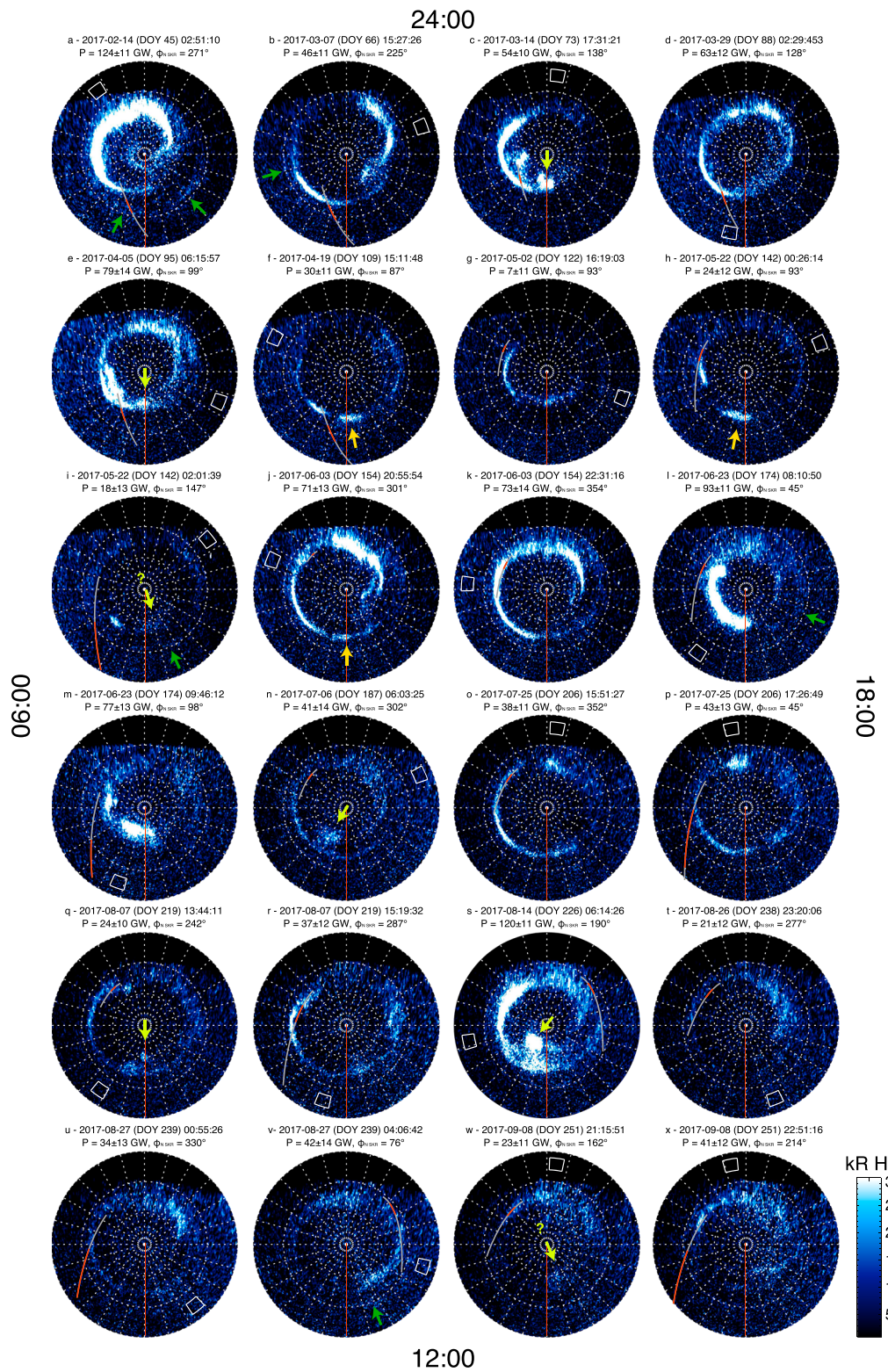
### 3.1. A Variety of Variable Components

Figure 1 displays polar projections of all STIS images, labelled a to x, versus LT. Images h-i, j-k, l-m, o-p, q-r, t-v, and w-x were acquired along successive HST orbits. The observations reveal diverse aurorae with highly variable, down to timescales of minutes (see Figure S1 and Movie S1), localized features dominated in intensity by the main oval. The latter is an inhomogeneous circumpolar ring generally more intense at dawn and premidnight. The quiet oval is quasi-circular at  $72\text{--}73^\circ$  latitude (images n and u-v) with brightnesses reaching a few tens of kR. Whenever active, it reaches higher latitudes (up to  $87\text{--}88^\circ$  in image a), often with a left-handed spiral shape (the oval develops counterclockwise from the pole). The brightest emissions exceed 150 kR (images a, l, and s). Overall, half of the STIS images were acquired when the Cassini magnetic footprint simultaneously intercepted aurora (red curves).

Isolated features regularly observed near noon poleward of the main oval (yellow arrows) or along it (orange arrows) are then interpreted as cusp aurorae. In the latter case, this interpretation is not unambiguous as hot spots subcorotating along the main oval can move through noon from dawn to dusk (Meredith et al., 2013). These events are often associated with duskside bifurcations of the main oval toward high latitudes (images b, e, j-k, n, s, and x) accounting for the general left-handed spiral shape of the main emission. The association between bifurcations, suggesting dynamical lobe reconnection, and noon spots strengthens their interpretation as cusp emissions. Image s shows the brightest example around 10:30 LT at  $84^\circ$  latitude, persisting over 44 min and variable at timescales of minutes (see Movie S1 and Figure S1) with unusual brightnesses  $\geq 100$  kR, the largest ever reported.

A faint dayside oval equatorward of the main one appears in several images (a, b, l, v, green arrows) within  $65\text{--}72^\circ$  latitude, sometimes in restricted LT sectors. While this secondary emission is distinct from the main one, we cannot exclude that it is reminiscent of ancient long-lived structures of the main oval which moved toward lower latitudes. Half of these examples correspond to active events when the main oval shifted to high latitudes. In image a, this secondary oval appears at  $69\text{--}72^\circ$  from 06:00 LT (or 00:00 LT  $\leq 70^\circ$ ) to 18:00 LT, with peak brightnesses  $\sim 10$  kR. Interestingly, during this exposure, Cassini intercepted the secondary oval near 11:00 LT during which MAGnetometer (MAG) measurements (Dougherty et al., 2004) of the azimuthal magnetic component (supporting information Figure S2) reveal successive small-scale abrupt gradients consistent with field-aligned current signatures, preceded  $\sim 1$  hr earlier by a large positive gradient indicating a strong upward current layer associated with the poleward main emission (e.g., Bunce et al., 2008; Hunt et al., 2014; Lamy et al., 2018; Talboys et al., 2009, 2011).

Finally, we could (still) not detect any Enceladus footprint (white boxes).



**Figure 1.** (a–x) Polar projections of HST/STIS images of northern Kronian aurorae in 2017 versus LT (red meridian = noon), projected at 1,100-km altitude, with light travel-corrected observing time, northern SKR phase, and total power radiated in the H<sub>2</sub> bands above each image. Yellow (orange) arrows indicate plausible cusp emissions poleward of (along) the main oval. Green arrows indicate low-latitude emission. White boxes indicate the Enceladus magnetic footprint. The red (gray) curves plot the Cassini magnetic footprint during ( $\pm 2$  h aside) each HST exposure. HST = Hubble Space Telescope; STIS = Space Telescope Imaging Spectrograph; SKR = Saturn’s Kilometric Radiation.

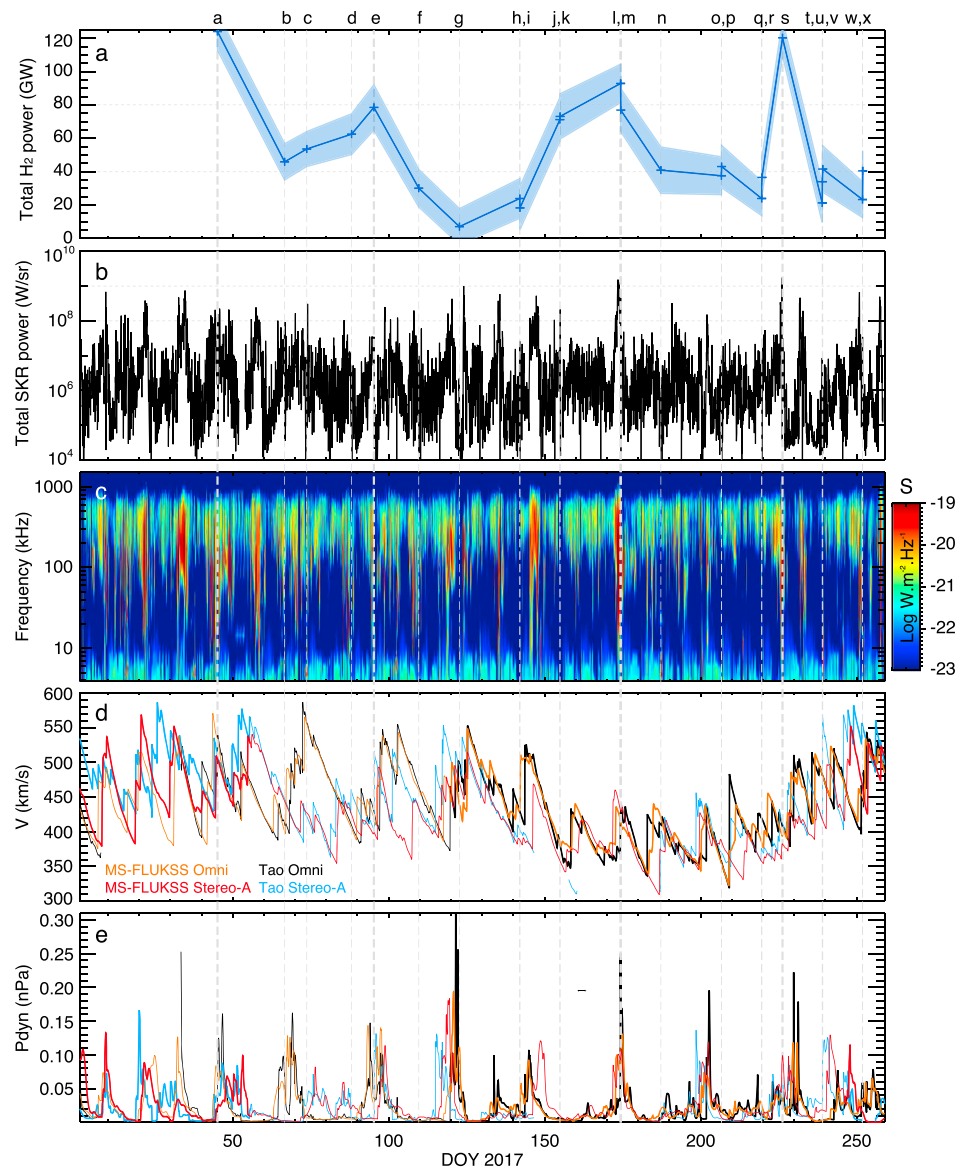


**Figure 2.** (a) Total auroral power radiated in the H<sub>2</sub> bands. (b) Total SKR power over 10–1100 kHz at 90-s resolution derived from (c) Cassini/RPWS dynamic spectrum of spectral flux density. (d, e) Velocity and dynamic pressure propagated at Saturn by two MHD models, using either Wind or Stereo-A data inputs. Boldface portions indicated angular separation between Wind/Stereo-A and Saturn  $\leq 90^\circ$ . The double black arrow plots a  $\pm 35$ -hr error bar. SKR = Saturn’s kilometric radiation; RPWS = Radio and Plasma Wave Science; MHD = magnetohydrodynamic.

### 3.2. Transient Enhancements and Associated Drivers

Figure 2a plots the total auroral power radiated by H<sub>2</sub> as a function of time, the individual power values being listed in Figure 1. Overall, the auroral power strongly varies with time, with a factor of  $\sim 10$  between extremal values, weeks apart (s-t), and with a factor of  $\sim 2$  between consecutive orbits (t-v or w-x). Seven events showing active aurorae radiated power  $\geq 65$  GW, up to 124, 93 and  $120 \pm 11$  GW for images a, l, and s, respectively. The latter includes the brightest cusp emission, which radiated  $13 \pm 0.5$  GW.

SW and planetary rotation both control SKR activity and UV aurorae. While SW-induced magnetospheric compressions trigger global SKR enhancement extending toward low frequencies and lasting for more than a planetary rotation (Bunce et al., 2010; Desch, 1982; Kurth et al., 2005, 2016; Lamy et al., 2010), short-lasting SKR intensifications phased with regular SKR bursts are associated with rotationally modulated nightside injections (Jackman et al., 2009; Lamy et al., 2013; Mitchell et al., 2009; Reed et al., 2018).

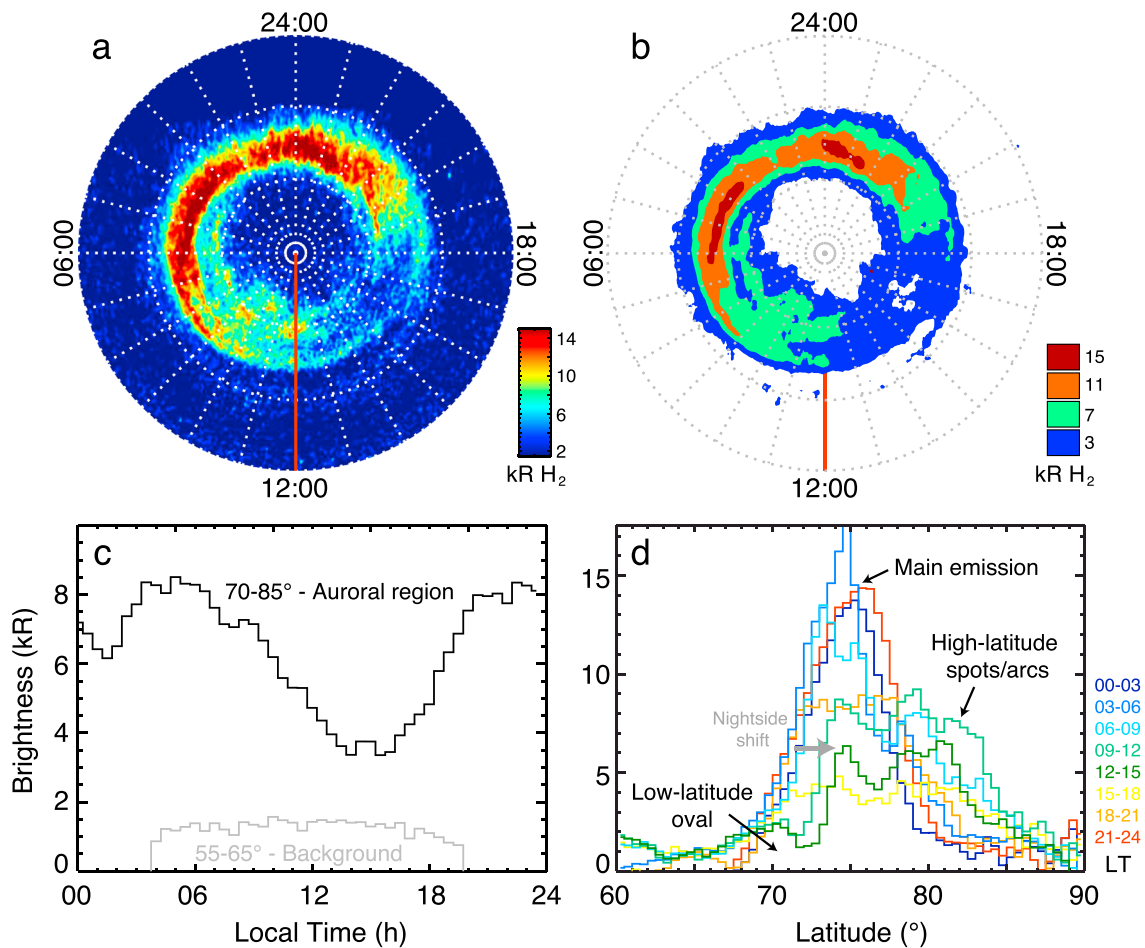


**Figure 3.** (a) Average of the 24 polar projections of Figure 1 smoothed with a 3 pix-wide running box. (b) Same as (a) but smoothed with a 17 pix-wide box instead to increase the signal-to-noise ratio, with isocontours at 3, 7, 11, and 15 kR. Both panels display the average locus and brightness of the circumpolar main oval within 70–85° latitude, of high-latitude emissions near noon and of a dayside secondary oval near 70°. (c) Average intensity profiles within 70–85° latitude (black line, aurora) and 55–65° (gray line, background) versus LT. The auroral intensity peaks at 05:00 and 22:00 LT. (d) Same as (c) versus latitude for successive 2-hr-wide (colored) LT ranges. The main emission is visible at all LT, with distinct high- and low-latitude emissions mostly visible on the dayside. LT = local time.

The purpose of Figure 2 is to assess the origin of the most active aurorae. Figures 2b and 2c display measurements of SKR power and spectral flux density, which quasi-continuously probe the auroral activity at 90-s resolution. Figures 2d and 2e display SW velocity and dynamic pressure propagated at Saturn. Vertical dashed lines mark the HST observations a–x. We first notice that most of (if not all) long-lasting SKR intensifications with low-/high-frequency extensions fairly match a SW pressure front within error bars. The five brightest events a, e, l-m, and s (boldface dashed lines), with power  $\geq 75$  GW, peak brightnesses  $\geq 150$  kR, and high-latitude emissions, all coincide with such SKR enhancements (see high-resolution dynamic spectra in supporting information Figure S3) and can therefore be identified as SW-driven auroral storms. Precisely, the UV observations were, respectively, acquired  $\sim 23, 19, 28-30,$  and  $20$  hr after the rise of SKR activity which, respectively, lasted for  $\geq 52, 22, 47,$  and  $32$  hr with multiple bursts, so that the HST images diagnosed a late stage of four different storms.

In contrast, the two consecutive images j-k, radiating  $\sim 70$  GW with peak brightnesses  $\geq 80$  kR, reveal a main emission confined at usual latitudes with a midnight active region which rotated toward dawn. These were acquired during quiet SW conditions at northern SKR phases of  $301^\circ$  and  $354^\circ$ , just before a modest northern SKR burst (see supporting information Figure S3) roughly consistent with the arrival of the active region to dawn. The auroral episodes j-k thus suggest a rotationally driven nightside injection.

### 3.3. Average Aurora at Solstice

We now turn to the mean spatial distribution and intensity of Saturn’s northern FUV aurorae. Figures 3a and 3b display average polar projections versus LT. Figures 3c and 3d display average intensity profiles versus LT and

latitude. The average main oval is a circumpolar ring of emissions of a few kR confined within 70–80° latitudes. Increasing brightnesses then gradually map to a dusk-to-noon partial ring, with the brightest emissions (15-kR isocontour in panel b) between premidnight and dawn.

The main oval expands poleward beyond  $\sim 80^\circ$  between 04:00 and 21:00 LT, encompassing polar arcs and spots produced by dawnside auroral storms, noon cusp, and duskside bifurcations. The low average brightness of these high-latitude emissions illustrates their transient nature. Figures 3a, 3b, and 3d additionally reveal a nightside shift of the main oval (gray arrow in Figure 3d): while the low-latitude boundary extends down to 70–72° on the nightside, it reaches 73–75° instead between 09:00 and 15:00 LT, with highest latitudes at 14:00 LT.

This shift enables us to identify a distinct LT-extended equatorward secondary oval within 67–73° in Figures 3a, 3b, and 3d, split from the main oval, with a typical mean brightness of  $\sim 2$  kR, occasionally exceeding 3 kR (the standard deviation per pixel in Figures 3a and 3b is  $\leq 1.5$  kR). It is pretty remarkable that this secondary oval is detected quasi-continuously from noon to dawn and dusk with roughly homogeneous intensities, which suggest that it primarily consists of steady weak emissions. These characteristics match the 1.7-kR secondary oval previously detected at  $-67^\circ$  nightside latitude. When considering the  $2^\circ$  northern latitudinal shift due to the northern magnetic field offset, the northern dayside oval appears at slightly higher latitudes than the nightside southern one, in agreement with the nightside shift of the main noticed above.

Figure 3c quantifies the LT dependence of northern aurorae discussed above by plotting the average brightness profile over 70–85° latitude (black line), a region fully visible at all LT, versus LT. It displays two distinct peaks at 05:00 and 22:00 LT. When building the same figure without SW-driven auroral storms, these peaks appear at 06:30 and 20:30 LT instead.

Finally, we similarly investigated the role of planetary rotation, previously found to modulate both the intensity and position of the main oval in both hemispheres (Nichols, Cecconi, et al., 2010; Nichols, Cowley, & Lamy, 2010). Supporting information Figure S4 displays the average brightness over 70–80° latitude for each image versus northern SKR phase and LT. The dashed line displays a guide meridian indicating an active auroral region rotating at the northern SKR period and reaching 06:00 LT at a phase of  $0^\circ$  (when SKR bursts occur). No active region can be continuously tracked along or close to this guide meridian, in contrast with previous positive results obtained in the Southern Hemisphere (Lamy, 2011; Lamy et al., 2013; Nichols, Cecconi, et al., 2010). Supporting information Figures S5a and S5b display average polar projections similar to Figures 3a and 3b but versus northern SKR phase. The LT were transposed into phases by again assuming that SKR maxima occur at the pass of a rotating active region through 06:00 LT. There is no maximum near  $0^\circ$ , in agreement with Figure S4. The two maxima observed near  $90^\circ$  and  $180^\circ$  instead mainly result from the SW-driven auroral storms. Interestingly, the low-latitude boundary of the main emission (e.g., 7 kR isocontour in Figure S5b) clearly reaches higher latitudes on the left-hand side (74–75° latitude at  $90^\circ$  phase) than on the right-hand side (72–73° latitude at  $180^\circ$  phase). This latitudinal shift is roughly consistent with that predicted from the tilt of the northern oval when the upward current layer reaches dawn (Nichols, Cowley, & Lamy, 2010) and therefore suggests a rotational control of the oval's position and not of its intensity, as already observed between 2011 and 2013 (Nichols et al., 2016).

#### 4. Discussion

In the previous section, we described the individual and average properties of the kronian northern aurorae at solstice, some of which are further discussed below.

The peak of northern average auroral brightness at 05:00 LT matches that previously seen with Cassini/UVIS observations (Carbary, 2012), although its displacement toward 06:30 when removing the auroral storms provides a typical uncertainty linked to the statistics of the data set. This may account for the discrepancy between the southern average auroral brightness peak observed by HST STIS/ACS at 09:00 (Lamy et al., 2009) and by Cassini/UVIS at 06:00 LT (Carbary, 2012). More importantly, the HST observations of 2017 additionally reveal a second peak of comparable amplitude at 20:30–22:00 LT, previously unreported, and strikingly reminiscent of Earth's aurora. This LT sector is also the one where the equatorward latitude of the main oval minimizes ( $\geq 3$  kR isocontours in Figure 3b). This secondary peak may thus arise either from a better viewing of the nightside sector or from more frequent nightside injections than previously observed, possibly favored under solstice conditions.

In contrast with a clear LT dependence of the auroral intensity, the rotational dynamics do not seem to play a significant role, if we except the moderate brightening phased with the northern SKR seen in the two successive images j-k and clues of a rotational control of the oval's position. Instead, the most obvious variability is that induced by large-scale auroral storms driven by the SW, for which SKR quasi-continuous observations provide total durations estimated between 22 and 48 hr at least. This largely exceeds the 11–21 hr range previously inferred by (Meredith et al., 2013), which explained a typical duration of  $\sim 1.5$  planetary rotations for the time needed by hot plasma injected from the nightside with a 60% subcorotational motion to complete one rotation. Accounting for the observed durations would imply very low subcorotational rates (from 20% to 50%). Instead, we propose that storms generally do not result from a single magnetospheric compression but from a series of them consistent with the multiple SKR bursts observed along each long event. The peculiar spiral shape observed in image a with extremely high latitudes surrounding the northern magnetic pole finally questions the interpretation of the main emission as a tracer of the open-closed field line boundary located  $1-2^\circ$  poleward, in which case the polar cap would correspond to a very small region around the pole. Analyzing Cassini in situ measurements obtained a few hours before image a, when the spacecraft sampled the dawnside region poleward of the main oval, is required to address this question. The detailed study of another example of SW-driven UV auroral storm temporally resolved by Cassini/UVIS with a concurrent SKR long-lasting enhancement is the subject of a companion paper (Palmaerts et al., 2018).

The apparent systematic  $\sim 3^\circ$  nightside shift in latitude of the average northern auroral oval, previously unreported to our knowledge, is consistent with the modeled influence of the SW flow on the open-closed field line boundary (Belenkaya et al., 2008).

Cusp emissions and bifurcations were observed very frequently, in  $\sim 50\%$  of the images. This unusually high occurrence rate is likely related to the magnetosphere/SW configuration reached at solstice. This scenario implies enhanced SW-driven mass loading of the magnetosphere and therefore supports more frequent nightside plasmoid releases/injections. The observation of an unusually bright cusp emission in image s, extended by a duskside bifurcation connecting it to a spiral-shaped main oval and observed during an auroral storm, suggests that it may have been induced by a SW-driven magnetospheric compression as regularly at Earth (Farrugia et al., 1995) and similarly proposed at Uranus (Lamy et al., 2017).

The novel identification of a dayside low-latitude emission with 2–3 kR brightnesses on average (which compare to that previously identified with comparable brightness and latitude on the nightside) implies a steady mechanism able to operate at all longitudes. In addition, it is worth noting that the dayside portion of the oval is not seen in all individual images and in half of the cases during auroral storms. This suggests an additional transient activity possibly linked to dayside compression of magnetic field lines. The previously proposed origin of such emission related to a suprathermal population of electrons in the middle magnetosphere (Grodent et al., 2010) is called into question by both this transient activity and by in situ magnetic measurements consistent with small-scale field-aligned currents. These features are alternatively consistent with either ancient long-lived structures of the main emission associated with strong field-aligned currents which moved toward lower latitudes or auroral precipitations associated with a secondary current system previously observed within  $68.5-72^\circ$  latitudes (Hunt et al., 2015). The detailed analysis of Cassini plasma measurements during this peculiar event is necessary to address this question.

## 5. Conclusion

In this study, we analyzed 24 HST/STIS images of Saturn's northern aurorae acquired throughout 2017 during northern summer solstice, concurrently with Cassini/RPWS observations of SKR and numerically propagated SW parameters. The observed northern aurorae display highly variable auroral components, with a total power ranging from 7 to 124 GW. The prominent component is the main oval observed poleward of  $72^\circ$  and shifted by  $\sim 3^\circ$  toward the nightside which bears clear signatures of the SW (four auroral storms coincident with SKR long-lasting enhancements) and planetary rotation (one auroral brightening coincident with a regular SKR burst). Recurrent cusp emissions and bifurcations are unexpectedly frequent, in 50% of the images, with an unusually bright cusp emission observed during an auroral storm which radiated  $13 \pm 1$  GW, likely triggered by the SW. The identification of a dayside secondary oval at  $70^\circ$  latitudes, 2–3 kR bright on average with some clues of temporal variability, brings new constraints to its possible origins. On average, the northern solstice aurorae display a strong LT dependence with two maxima at dawn and premidnight, the latter being attributed to regular nightside injections, with clues of a rotational control of the oval's average

position but not of its intensity. These results provide a reference frame to analyze Cassini in situ measurements, whether simultaneous (the Cassini footprints intercepted an auroral component in half of the images) or not.

### Acknowledgments

The UV observations were obtained from the ESA/NASA Hubble Space Telescope (GO program 14811): the original data can be retrieved from the MAST archive and the processed data from the APIS service hosted by the Paris Astronomical Data Centre at <http://apis.obspm.fr>. The Cassini/RPWS and MAG original data are accessible through the PDS archive at <https://pds.nasa.gov/>. The HFR processed data are available through the LESIA/Kronos database at <http://www.lesia.obspm.fr/kronos>. L. L. thanks Linda Spilker for her support to the original HST proposal, Fannie Serrano and Pauline Richard, who investigated short-term dynamics of Saturn's aurorae during their internship at LESIA, and Gabby Provan for useful discussions on the inexhaustible topic of Kronian magnetospheric periodicities. The French coauthors acknowledge support from CNES and CNRS/INSU programs of Planetology (PNP) and Heliophysics (PNST). S. V. B. was supported by an STFC Ernest Rutherford Fellowship ST/M005534/1. The research at the University of Iowa was supported by NASA through contract 1415150 with the Jet Propulsion Laboratory.

### References

- Badman, S. V., Branduardi-Raymont, G., Galand, M., Hess, S. L. G., Krupp, N., Lamy, L., et al. (2015). Auroral processes at the giant planets: Energy deposition, emission mechanisms, morphology and spectra. *Space Science Reviews*, *187*, 99–179. <https://doi.org/10.1007/s11214-014-0042-x>
- Belenkaya, E. S., Cowley, S. W. H., Badman, S. V., Blokhina, M. S., & Kalegaev, V. V. (2008). Dependence of the open-closed field line boundary in Saturn's ionosphere on both the IMF and solar wind dynamic pressure: Comparison with the UV auroral oval observed by the HST. *Annales Geophysicae*, *26*, 159–166. <https://doi.org/10.5194/angeo-26-159-2008>
- Bunce, E. J., Arridge, C. S., Clarke, J. T., Coates, A. J., Cowley, S. W. H., Dougherty, M. K., et al. (2008). Origin of Saturn's aurora: Simultaneous observations by Cassini and the Hubble Space Telescope. *Journal of Geophysical Research*, *113*, A09209. <https://doi.org/10.1029/2008JA013257>
- Bunce, E., Cowley, S. W. H., Talboys, D. L., Dougherty, M. K., Lamy, L., Kurth, W. S., et al. (2010). Extraordinary field-aligned current signatures in Saturn's high-latitude magnetosphere: Analysis of Cassini data during Revolution 89. *Journal of Geophysical Research*, *115*, A10238. <https://doi.org/10.1029/2010JA015612>
- Carbary, J. F. (2012). The morphology of Saturn's ultraviolet aurora. *Journal of Geophysical Research*, *117*, A06210. <https://doi.org/10.1029/2012JA017670>
- Clarke, J. T., Gérard, J.-C., Grodent, D., Wannawichian, S., Gustin, J., Connerney, J., et al. (2005). Morphological differences between Saturn's ultraviolet aurorae and those of Earth and Jupiter. *Nature*, *433*, 717–719. <https://doi.org/10.1038/nature03331>
- Clarke, J. T., Nichols, J., Gérard, J., Grodent, D., Hansen, K. C., Kurth, W., et al. (2009). Response of Jupiter's and Saturn's auroral activity to the solar wind. *Journal of Geophysical Research*, *114*, A05210. <https://doi.org/10.1029/2008JA013694>
- Desch, M. D. (1982). Evidence for solar wind control of Saturn radio emission. *Journal of Geophysical Research*, *87*(A6), 4549–4554. <https://doi.org/10.1029/JA087iA06p04549>
- Dougherty, M. K., Kellock, S., Southwood, D. J., Balogh, A., Smith, E. J., Tsurutani, B. T., et al. (2004). The Cassini magnetic field investigation. *Space Science Reviews*, *114*, 331–383. <https://doi.org/10.1007/s11214-004-1432-2>
- Farrugia, C. J., Sandholt, P. E., Cowley, S. W. H., Southwood, D. J., Egeland, A., Stauning, P., et al. (1995). Reconnection-associated auroral activity stimulated by two types of upstream dynamic pressure variations: Interplanetary magnetic field  $B_z \sim 0$ ,  $B_y \ll 0$  case. *Journal of Geophysical Research*, *100*(A11), 21,753–21,772. <https://doi.org/10.1029/95JA01082>
- Gérard, J.-C., Bunce, E. J., Grodent, D., Cowley, S. W. H., Clarke, J. T., & Badman, S. V. (2005). Signature of Saturn's auroral cusp: Simultaneous Hubble Space Telescope FUV observations and upstream solar wind monitoring. *Journal of Geophysical Research*, *110*, A11201. <https://doi.org/10.1029/2005JA011094>
- Grodent, D. (2015). A brief review of ultraviolet auroral emissions on giant planets. *Space Science Reviews*, *187*, 23–50. <https://doi.org/10.1007/s11214-014-0052-8>
- Grodent, D., Gustin, J., Gérard, J.-C., Radioti, A., Bonfond, B., & Pryor, W. R. (2011). Small-scale structures in Saturn's ultraviolet aurora. *Journal of Geophysical Research*, *116*, A09225. <https://doi.org/10.1029/2011JA016818>
- Grodent, D., Radioti, A., Bonfond, B., & Gérard, J.-C. (2010). On the origin of Saturn's outer auroral emission. *Journal of Geophysical Research*, *115*, A08219. <https://doi.org/10.1029/2009JA014901>
- Gurnett, D. A., Kurth, W. S., Kirchner, D. L., Hospodarsky, G. B., Averkamp, T. F., Zarka, P., et al. (2004). The Cassini radio and plasma wave investigation. *Space Science Reviews*, *114*, 395–463.
- Gustin, J., Grodent, D., Radioti, A., Pryor, W., Lamy, L., & Ajello, J. (2017). Statistical study of Saturn's auroral electron properties with Cassini/UVIS FUV spectral images. *Icarus*, *284*, 264–283. <https://doi.org/10.1016/j.icarus.2016.11.017>
- Hunt, G. J., Cowley, S. W. H., Provan, G., Bunce, E. J., Alexeev, I. I., Belenkaya, E. S., et al. (2014). Field-aligned currents in Saturn's southern nightside magnetosphere: Subcorotation and planetary period oscillation components. *Journal of Geophysical Research: Space Physics*, *119*, 9847–9899. <https://doi.org/10.1002/2014JA020506>
- Hunt, G. J., Cowley, S. W. H., Provan, G., Bunce, E. J., Alexeev, I. I., Belenkaya, E. S., et al. (2015). Field-aligned currents in Saturn's northern nightside magnetosphere: Evidence for interhemispheric current flow associated with planetary period oscillations. *Journal of Geophysical Research: Space Physics*, *120*, 7552–7584. <https://doi.org/10.1002/2015JA021454>
- Jackman, C. M., Lamy, L., Freeman, M. P., Zarka, P., Ceconi, B., Kurth, W. S., et al. (2009). On the character and distribution of lower-frequency radio emissions at Saturn and their relationship to substorm-like events. *Journal of Geophysical Research*, *114*, A08211. <https://doi.org/10.1029/2008JA013997>
- Kim, T. K., Pogorelov, N. K., Zank, G. P., Elliott, H. A., & McComas, D. J. (2016). Modeling the solar wind at the Ulysses, Voyager, and New Horizons Spacecraft. *The Astrophysical Journal*, *832*(1), 72. <https://doi.org/10.3847/0004-637X/832/1/72>
- Kimura, T., Lamy, L., Tao, C., Badman, S. V., Kasahara, S., Ceconi, B., et al. (2013). Long-term modulations of Saturn's auroral radio emissions by the solar wind and seasonal variations controlled by the solar ultraviolet flux. *Journal of Geophysical Research: Space Physics*, *118*, 7019–7035. <https://doi.org/10.1002/2013JA018833>
- King, J. H., & Papitashvili, N. E. (2005). Solar wind spatial scales in and comparisons of hourly Wind and ACE plasma and magnetic field data. *Journal of Geophysical Research*, *110*, A02104. <https://doi.org/10.1029/2004JA010649>
- Kinrade, J., Badman, S. V., Bunce, E. J., Tao, C., Provan, G., Cowley, S. W. H., et al. (2017). An isolated, bright cusp aurora at Saturn. *Journal of Geophysical Research: Space Physics*, *122*, 6121–6138. <https://doi.org/10.1002/2016JA023792>
- Kurth, W. S., Bunce, E. J., Clarke, J. T., Cray, F. J., Grodent, D. C., Ingersoll, A. P., et al. (2009). Auroral processes. In M. K. Dougherty, L. W. Esposito, & S. M. Krimigis (Eds.), *Saturn from Cassini-Huygens*. Berlin, Allemagne: Springer, pp. 333–374.
- Kurth, W. S., Gurnett, D. A., Clarke, J. T., Zarka, P., Desch, M. D., Kaiser, M. L., et al. (2005). An Earth-like correspondence between Saturn's auroral features and radio emission. *Nature*, *433*, 722–725. <https://doi.org/10.1038/nature03334>
- Kurth, W. S., Hospodarsky, G. B., Gurnett, D. A., Lamy, L., Dougherty, M. K., Nichols, J., et al. (2016). Saturn kilometric radiation intensities during the Saturn auroral campaign of 2013. *Icarus*, *263*, 2–9. <https://doi.org/10.1016/j.icarus.2015.01.003>
- Lamy, L. (2011). Variability of southern and northern SKR periodicities. In H. O. Rucker, et al. (Eds.), *Planetary radio emissions, V II*. Vienna: Austrian Academy of Sciences Press, pp. 39–50.
- Lamy, L. (2017). The Saturnian kilometric radiation before the Cassini Grand Finale. In G. Fischer, et al. (Eds.), *Planetary radio emissions, V III*. Vienna: Austrian Academy of Sciences Press, pp. 171–190.

- Lamy, L., Cecconi, B., Prangé, R., Zarka, P., Nichols, J. D., & Clarke, J. T. (2009). An auroral oval at the footprint of Saturn's kilometric radio sources, collocated with the UV aurorae. *Journal of Geophysical Research*, *114*, A10212. <https://doi.org/10.1029/2009JA014401>
- Lamy, L., Prangé, R., Hansen, K. C., Tao, C., Cowley, S. W. H., Stallard, T. S., et al. (2017). The aurorae of Uranus past equinox. *Journal of Geophysical Research: Space Physics*, *122*, 3997–4008. <https://doi.org/10.1002/2017JA023918>
- Lamy, L., Prangé, R., Pryor, W., Gustin, J., Badman, S. V., Melin, H., et al. (2013). Multispectral simultaneous diagnosis of Saturn's aurorae throughout a planetary rotation. *Journal of Geophysical Research: Space Physics*, *118*, 4817–4843. <https://doi.org/10.1002/jgra.50404>
- Lamy, L., Schippers, P., Zarka, P., Cecconi, B., Arridge, C. S., Dougherty, M. K., et al. (2010). Properties of Saturn kilometric radiation measured within its source region. *Geophysical Research Letters*, *37*, L12104. <https://doi.org/10.1029/2010GL043415>
- Lamy, L., Zarka, P., Cecconi, B., Prangé, R., Kurth, W. S., & Gurnett, D. A. (2008). Saturn kilometric radiation: Average and statistical properties. *Journal of Geophysical Research*, *113*, A07201. <https://doi.org/10.1029/2007JA012900>
- Lamy, L., Zarka, P., Cecconi, B., Prangé, R., Kurth, W. S., Hospodarsky, G., et al. (2018). The low frequency source of Saturn's Kilometric Radiation. *Science*. <https://doi.org/10.1126/science.aat2027>
- Meredith, C. J., Alexeev, I. I., Badman, S. V., Belenkaya, E. S., Cowley, S. W. H., Dougherty, M. K., et al. (2014). Saturn's dayside ultraviolet auroras: Evidence for morphological dependence on the direction of the upstream interplanetary magnetic field. *Journal of Geophysical Research: Space Physics*, *119*, 1994–2008. <https://doi.org/10.1002/2013JA019598>
- Meredith, C. J., Cowley, S. W. H., Hansen, K. C., Nichols, J. D., & Yeoman, T. K. (2013). Simultaneous conjugate observations of small-scale structures in Saturn's dayside ultraviolet auroras: Implications for physical origins. *Journal of Geophysical Research: Space Physics*, *118*, 2244–2266. <https://doi.org/10.1002/jgra.50270>
- Meredith, C. J., Cowley, S. W. H., & Nichols, J. D. (2014). Survey of Saturn auroral storms observed by the Hubble Space Telescope: Implications for storm time scales. *Journal of Geophysical Research: Space Physics*, *119*, 9624–9642. <https://doi.org/10.1002/2014JA020601>
- Mitchell, D. G., Krimigis, S. M., Paranicas, C., Brandt, P. C., Carbary, J. F., Roelof, E. C., et al. (2009). Recurrent energization of plasma in the midnight-to-dawn quadrant of Saturn's magnetosphere, and its relationship to auroral UV and radio emissions. *Planetary and Space Science*, *57*, 1732–1742. <https://doi.org/10.1016/j.pss.2009.04.002>
- Nichols, J. D., Badman, S. V., Bunce, E. J., Clarke, J. T., Cowley, S. W. H., Hunt, G. J., & Provan, G. (2016). Saturn's northern auroras as observed using the Hubble Space Telescope. *Icarus*, *263*, 17–31. <https://doi.org/10.1016/j.icarus.2015.09.008>
- Nichols, J. D., Cecconi, B., Clarke, J. T., Cowley, S. W. H., Gérard, J.-C., Grotcott, A., et al. (2010). Variation of Saturn's UV aurora with SKR phase. *Geophysical Research Letters*, *37*, L15102. <https://doi.org/10.1029/2010GL044057>
- Nichols, J. D., Cowley, S. W. H., & Lamy, L. (2010). Dawn-dusk oscillation of Saturn's conjugate auroral ovals. *Geophysical Research Letters*, *37*, L24102. <https://doi.org/10.1029/2010GL045818>
- Palmaerts, B., Radioti, A., Roussos, E., Grodent, D., Gérard, J.-C., Krupp, N., & Mitchell, D. G. (2016). Pulsations of the polar cusp aurora at Saturn. *Journal of Geophysical Research: Space Physics*, *121*, 11,952–11,963. <https://doi.org/10.1002/2016JA023497>
- Palmaerts, B., Radioti, A., Yao, Z. H., Bradley, T. J., Roussos, E., Lamy, L., et al. (2018). Auroral storm and polar arcs at Saturn—Final Cassini/UVIS auroral observations. *Geophysical Research Letters*, *45*. <https://doi.org/10.1029/2018GL078094>
- Pogorelov, N. V., Borovikov, S. N., Heerikhuisen, J., Tae, K. K., Kryukov, I. A., & Zank, G. P. (2014). MS-FLUKSS and its application to modeling flows of partially ionized plasma in the heliosphere. In *2014 Annual Conference on Extreme Science and Engineering Discovery Environment ACM Digital Library (New York)*. <https://doi.org/10.1145/2616498.2616499>
- Prangé, R., Pallier, L., Hansen, K. C., Howard, R., Vourlidis, A., Courtin, R., & Parkinson, C. (2004). An interplanetary shock traced by planetary auroral storms from the Sun to Saturn. *Nature*, *432*, 78–81. <https://doi.org/10.1038/nature02986>
- Pryor, W. R., Rymer, A. M., Mitchell, D. G., Hill, T. W., Young, D. T., Saur, J., et al. (2011). The auroral footprint of Enceladus on Saturn. *Nature*, *472*, 331–333. <https://doi.org/10.1038/nature09928>
- Radioti, A., Grodent, D., Gérard, J.-C., Milan, S. E., Bonfond, B., Gustin, J., & Pryor, W. (2011). Bifurcations of the main auroral ring at Saturn: ionospheric signatures of consecutive reconnection events at the magnetopause. *Journal of Geophysical Research*, *116*, A11209. <https://doi.org/10.1029/2011JA016661>
- Radioti, A., Grodent, D., Gérard, J.-C., Roussos, E., Mitchell, D., Bonfond, B., & Pryor, W. (2015). Auroral spirals at Saturn. *Journal of Geophysical Research: Space Physics*, *120*, 8633–8643. <https://doi.org/10.1002/2015JA021442>
- Radioti, A., Grodent, D., Gérard, J.-C., Roussos, E., Paranicas, C., Bonfond, B., et al. (2009). Transient auroral features at Saturn: Signatures of energetic particle injections in the magnetosphere. *Journal of Geophysical Research*, *114*, A03210. <https://doi.org/10.1029/2008JA013632>
- Radioti, A., Grodent, D., Yao, Z. H., Gérard, J.-C., Badman, S. V., Pryor, W., & Bonfond, B. (2017). Dawn auroral breakup at saturn initiated by auroral arcs: UVIS/Cassini beginning of grand finale phase. *Journal of Geophysical Research: Space Physics*, *122*, 12,111–12,119. <https://doi.org/10.1002/2017JA024653>
- Reed, J. J., Jackman, C. M., Lamy, L., Kurth, W. S., & Whiter, D. K. (2018). Low-frequency extensions of the Saturn kilometric radiation as a proxy for magnetospheric dynamics. *Journal of Geophysical Research: Space Physics*, *123*, 443–463. <https://doi.org/10.1002/2017JA024499>
- Talboys, D. L., Arridge, C. S., Bunce, E. J., Coates, A. J., Cowley, S. W. H., & Dougherty, M. K. (2009). Characterization of auroral current systems in Saturn's magnetosphere: High-latitude Cassini observations. *Journal of Geophysical Research*, *114*, A06220. <https://doi.org/10.1029/2008JA013846>
- Talboys, D. L., Bunce, E. J., Cowley, S. W. H., Arridge, C. S., Coates, A. J., & Dougherty, M. K. (2011). Statistical characteristics of field-aligned currents in Saturn's nightside magnetosphere. *Journal of Geophysical Research*, *116*, A04213. <https://doi.org/10.1029/2010JA016102>
- Tao, C., Kataoka, R., Fukunishi, H., Takahashi, Y., & Yokoyama, T. (2005). Magnetic field variations in the Jovian magnetotail induced by solar wind dynamic pressure enhancements. *Journal of Geophysical Research*, *110*, A11208. <https://doi.org/10.1029/2004JA010959>
- Zieger, B., & Hansen, K. C. (2008). Statistical validation of a solar wind propagation model from 1 to 10 AU. *Journal of Geophysical Research*, *113*, A08107. <https://doi.org/10.1029/2008JA013046>